The complex-formation behaviour of His residues in the fifth Cu^{2+} binding site of human prion protein: a close look†

Maurizio Remelli,*[a] Daniela Valensin,[b] Dimitri Bacco,[a] Ewa Gralka,[c] Remo Guerrini,[d] Caterina Migliorini[b] and Henryk Kozlowski[c]

Received (in Montpellier, France) 20th May 2009, Accepted 29th July 2009
First published as an Advance Article on the web 11th September 2009
DOI: 10.1039/b9nj00202b

Human Prion Protein ($hPrP^C$) is able to bind up to six Cu^{2+} ions. Four of them can be allocated in the "octarepeat domain", a region of the unstructured *N*-terminal domain containing four tandem-repetitions of the sequence PHGGGWGQ. It is widely accepted that the additional binding sites correspond to His-96 and His-111 residues. However, recent literature does not agree on the role and the behavior of these sites in Cu^{2+} complexation to $hPrP^C$. In order to shed more light on this topic, some peptidic analogues of the $PrP_{92–113}$ fragment were synthesized: (H96A)$PrP_{92–113}$, (H111A)$PrP_{92–113}$, (H96N^{τ}-Me-His)$PrP_{92–113}$, (H111N^{τ}-Me-His)$PrP_{92–113}$, (H96N^{τ}-Me-His)$PrP_{92–100}$, (H111N^{τ}-Me-His)$PrP_{106–113}$, where an alanine or a histidine methylated at the τ nitrogen atom of its imidazole ring have been substituted to His-96 or His-111. The first two ligands allowed to confirm that His-111 binding site is stronger than His-96 one: they act as independent sites even at Cu^{2+}-ion substoichiometric levels. Neither multi-histidine binding nor bis-complex formation has been detected at neutral pH. N^{τ} methylation gave evidence that τ nitrogens of imidazole residues can participate in complex-formation only at acidic pH, where displacement of amidic protons by Cu^{2+} ions is not allowed. Finally, the length of the fragment does not appear to have any significant influence on the behavior of the two His-96 and His-111 binding sites, from the point of view of either the coordination geometry or their relative strength.

Introduction

The prion protein (PrP^C) is a membrane-anchored glycoprotein,[1] highly expressed in the nervous system of mammals, birds, fish and amphibians. PrP^C plays a basic role in a class of neuro-degenerative diseases known as Transmissible Spongiform Encephalopathies (TSEs), also called prion diseases.[1] Among them, the well-known "mad cow disease", the Bovine Spongiform Encephalopathy,[2] caused a big concern in late 1980s due to its epidemic in UK and its successive discovery in many countries all over the world. Only few years later, a new variant of the human Creutzfeldt–Jakob disease was discovered,[3] leading to hypothesis of the prion transmission from animals to humans.[4] As a matter of fact, a peculiarity which distinguishes prion diseases from the other neurodegenerative diseases is that they can be infectious:[1,4] it is now widely accepted that the infectious agent is a protease-resistant isoform of PrP^C, named PrP^{Sc}. As a consequence, prion diseases can be provoked in regular animal models by inoculation or even by oral administration of PrP^{Sc},[4] and they can be studied more easily than other neurodegenerative disorders, like *e.g.* Alzheimer's or Parkinson's diseases.

In spite of the big interest in PrP^C, its biological function is not yet completely understood. However, its ability to bind Cu^{2+} ions is well accepted as well as its SOD-like activity.[5] These features suggest that PrP^C plays a foreground role in copper homeostasis.[6] It is well-known that PrP^C can bind four Cu^{2+} ions in the so-called "octarepeat domain",[7] a region of the protein close to the *N*-terminus and containing, in mammalian PrP^C, four tandem repetitions of the sequence PHGGGWGQ.[8] Similar repetitions are also present in fish[9] and avian PrP^C.[8] It is also accepted that PrP^C can bind additional Cu^{2+} ions outside the octarepeat region; the first evidence was given by Brown *et al.*[10] but it was only in 2001 that Jackson *et al.*[11,12] revealed that such "fifth" copper-coordination site was located around the His-96 and His-111 residues, a region involved in prion propagation.

Many spectroscopic studies have been devoted to the characterization of this Cu^{2+} binding site from the point of view of both its binding strength and coordination geometry,[13–28,] with somewhat controversial results. It is mostly accepted that at neutral pH the $PrP_{91–115}$ region is the strongest Cu^{2+} binding site of the protein,[14–16] involving the amidic nitrogens of polypeptidic backbone even at substoichiometric Cu^{2+} amounts.[22,23] Increasing the copper concentration, a multi-histidine species can be formed[19,22,23] similar to that found at

[a] *Dipartimento di Chimica, Università di Ferrara, via L. Borsari 46, 44100 Ferrara, Italia. E-mail: maurizio.remelli@unife.it; Fax: +39 0532 240709; Tel: +39 0532 455150*
[b] *Dipartimento di Chimica, Università di Siena, Via A. Moro 2, 53100 Siena, Italia*
[c] *Faculty of Chemistry, University of Wroclaw, F. Joliot-Curie 14, 50383 Wroclaw, Poland*
[d] *Dipartimento di Scienze Farmaceutiche, Università di Ferrara, via Fossato di Mortara 17/19, 44100 Ferrara, Italia*

† Electronic supplementary information (ESI) available: Tables S1–S3 and Figs. S1 and S2. See DOI: 10.1039/b9nj00202b

acidic pH[13,18] and for the octapeptide region.[20,21] Both His-96 and His-111 play a role in complexation, but it is not clear-cut if they bind the Cu^{2+} ion together[12,13,15,18] or independently with different binding strengths.[16,19,22,23,25,26] Two Met residues are present around His-111, at the positions 109 and 112. The sulfur atoms of their side chains could, in principle, participate in Cu^{2+} complexation, thus influencing the binding ability of this site, but it is not clear if it occurs[12,26] or not.[15] Finally, the hydrophobic region following His-111 in the hPrP sequence seems to affect neither the coordination geometry nor the donor-atom set[22,23,25] but, eventually, the preference between His-96 and His-111.[22]

In order to obtain the stoichiometry and the distribution of complex species formed at different pH or concentration values, solution-equilibria studies on peptidic models are the way of choice. They give conditional complex-formation constants which can be used (i) to compare the binding strength of different sites, (ii) to calculate the species distribution under given experimental conditions and (iii) to predict the competition with other ligands or metal ions. Since 2004, our research group have been using potentiometry, calorimetry and many spectroscopic techniques to investigate the Cu^{2+} binding equilibria at the "fifth" site of hPrP protein, exploring first the His-111 region[29–31] and then considering some hPrP fragments encompassing the entire 91–120 domain.[32] The pivotal role of imidazolic side chain of His in "anchoring" the metal was confirmed and NMR suggested the subsequent possibility of both the coordination directions, *i.e.* towards either the *N*-terminus (as usually found) or the *C*-terminus (like in the octarepeat domain). A study on a series of protected oligopeptides containing His at either their *C*- or the *N*-terminus[33] confirmed this possibility. The two coordination modes were found to differ only slightly in energy thus suggesting that, in long peptides, the influence of the adjacent amino acid residues can address the coordination towards either the *C*- or the *N*-terminus. Competition diagrams calculated from stability-constant suggested that the binding site located at His-96 is weaker than that located at His-111, in agreement with NMR results. The two binding sites proved independent: at substoichiometric Cu^{2+} concentrations, the $hPrP_{91–120}$ peptide binds a copper ion at one out of the two His sites, whereas di-nuclear species form when the metal is in excess.

Rizzarelli and co-workers applied combined equilibrium and spectroscopic methods to investigate the interaction of Cu^{2+} ion with the His-111, His-96 and His-187 containing domains.[34–38] They suggested 3N and 4N complexes containing deprotonated amide-N donors as the most abundant species at physiological pH, with a weak pH-dependent binding of the Met-109 residue for the 3N-coordinated complexes. Studying the $hPrP_{84–114}$ and $hPrP_{76–114}$ polypeptides they showed the preferential formation of macrochelates at acidic pH, while all the histidines can be considered as independent metal-binding sites at neutral pH, and the preference for Cu^{2+} binding follows the order: His-111 > His-96 >> His-77 ~ His-85.

It is clear from this literature overview that some points are still controversial: the relative Cu^{2+}-binding strength of the two His-96 and His-111 sites in hPrP; the possible formation of macrochelates in the presence of equimolar or substoichiometric amount of Cu^{2+} ions, at neutral pH, with a multi-histidine binding mode; the possible formation of bis-complexes when the ligand is in excess; the coordination direction (towards the *N*- or *C*-terminus) after the first anchoring to imidazole nitrogen. Unfortunately, NMR is unable to distinguish between the His-96 and His-111 residues in the same PrP fragment. In order to shed more light on the above topics, the following analogues for the fifth copper-binding site of human PrP^C were synthesized (see Table 1): (H96A)$PrP_{92–113}$, (H111A)$PrP_{92–113}$, (H96N^{τ}-Me-His)$PrP_{92–113}$, (H111N^{τ}-Me-His)-$PrP_{92–113}$, (H96N^{τ}-Me-His)$PrP_{92–100}$, (H111N^{τ}-Me-His)-$PrP_{106–113}$, where alanine or histidine methylated at the τ nitrogen atom of its imidazole ring (see Fig. 1) have been substituted to His-96 or His-111. The study has been carried out in aqueous solution and in a wide pH range, at I = 0.1 M and T = 298.2 K. Protonation and complex-formation constants have been potentiometrically determined; formation enthalpies have been measured by direct solution calorimetry; complex-formation model and species stoichiometry have been carefully checked by means of UV-VIS absorption, CD, EPR and NMR spectroscopies. Structural hypotheses on the main complex species are suggested.

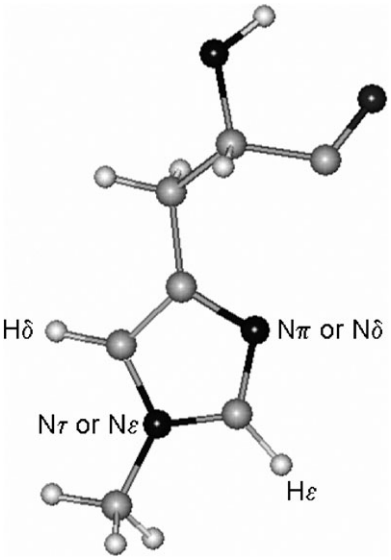

Fig. 1 Structure of N^{τ}-Me-L-histidine

Experimental

Peptide synthesis

General information. Amino acids, protected amino acids, resin for solid-phase synthesis and chemicals were purchased from Bachem, Novabiochem or Fluka. H-His(N^{τ}-Me)-OH was Fmoc protected following procedures reported in literature.[39]

General procedures for the solid phase peptide synthesis. All peptides were synthesised using Fmoc/t-butyl chemistry with a Syro XP multiple peptide synthesizer (MultiSynTech GmbH, Witten, Germany). As an illustrative example the synthesis of (H96A)$PrP_{92–113}$ is described. 4-(2′,4′-Dimethoxyphenyl-Fmoc-aminomethyl)phenoxyacetamidonorleucyl–MBHA resin (Rink Amide MBHA resin) (0.38 mmol g^{-1}, 0.2 g), was treated

Table 1 List of peptide sequences considered for Cu^{2+} binding studies

(H96A)$PrP_{92–113}$	(Ac-GGGT**A**SQWNKPSKPKTNMK**H**MA-NH_2)
(H111A)$PrP_{92–113}$	(Ac-GGGT**H**SQWNKPSKPKTNMK**A**MA-NH_2)
(H96N$^{\tau}$-Me-His)$PrP_{92–113}$	(Ac-GGGT-N$^{\tau}$**MeH**-SQWNKPSKPKTNMK**H**MA-NH_2)
(H111N$^{\tau}$-Me-His)$PrP_{92–113}$	(Ac-GGGT**H**SQWNKPSKPKTNMK-N$^{\tau}$**MeH**-MA-NH_2)
(H96N$^{\tau}$-Me-His)$PrP_{92–100}$	(Ac-GGGT-N$^{\tau}$**MeH**-SQWN-NH_2)
(H111N$^{\tau}$-Me-His)$PrP_{106–113}$	(Ac-KTNMK-N$^{\tau}$**MeH**-MA-NH_2)

with 40% piperidine/*N*,*N*-dimethylformamide (DMF) and linked with Fmoc-Ala-OH by using [*O*-(7-azabenzotriazol-1-yl)-1,1,3,3-tetramethyluronium hexafluorophosphate] (HATU) as the coupling reagent. The following N^{α}-Fmoc amino acids were sequentially coupled to the growing peptide chain: Fmoc-Met-OH, Fmoc-His(Boc)-OH, Fmoc-Lys(Boc)-OH, Fmoc-Met-OH, Fmoc-Asn(Trt)-OH, Fmoc-Thr(tBu)-OH, Fmoc-Lys(Boc)-OH, Fmoc-Pro-OH, Fmoc-Lys(Boc)-OH, Fmoc-Ser(tBu)-OH, Fmoc-Pro-OH, Fmoc-Lys(Boc)-OH, Fmoc-Asn(Trt)-OH, Fmoc-Trp(Boc)-OH, Fmoc-Gln(Trt)-OH, Fmoc-Ser(tBu)-OH, Fmoc-Ala-OH, Fmoc-Thr(tBu)-OH, Fmoc-Gly-OH, Fmoc-Gly-OH, Fmoc-Gly-OH. All the N^{α}-Fmoc amino acids (4 equiv.) were coupled to the growing peptide chain by using HATU (4 equiv.) in DMF in the presence of an equimolar concentration of 4-methylmorpholine (NMM), and the coupling reaction time was 1 h. To improve the analytical profile of the crude peptide, capping with acetic anhydride (0.5 M in DMF) with the presence of NMM (0.25 M in DMF) (3 : 1 v/v; 2 mL/0.2 g of resin) was performed at any step. 40% Piperidine–DMF was used to remove the Fmoc group at every step. After the removal of the last *N*-terminal Fmoc group, a capping cycle was performed to introduce a *N*-terminal acetyl group. The peptide resin was washed with methanol and dried *in vacuo* to yield the protected peptide resin. The other peptides were synthesised in a similar manner. The protected peptide resin was treated with reagent B[40] (trifluoroacetic acid (TFA)–H_2O–phenol–triisopropylsilane 88 : 5 : 5 : 2; v/v; 10 mL/0.2 g of resin) for 2 h at room temperature. After filtration of the resin, the solvent was concentrated *in vacuo* and the residue triturated with ether. The crude peptide was purified by preparative reversed-phase HPLC to yield a white powder after lyophilization.

Peptide purification and analytical determinations. Preparative HPLC instrumentation consisted in a Delta Prep 4000 system (Waters, Milford, MA, USA) equipped with a Jupiter column C_{18} (250 × 30 mm, 300 A, 15 μm spherical particle size). The column flow-rate was 25 mL min^{-1} with a mobile phase containing solvent A (10%, v/v, acetonitrile in 0.1% TFA), and a linear gradient from 0 to 40% of solvent B (60%, v/v, acetonitrile in 0.1% TFA) over 25 min for the elution of peptides. Analytical HPLC analyses were performed on a Beckman 116 liquid chromatograph equipped with a Beckman 166 diode array detector. Analytical purity of the peptides were determined using a Nucleodur C_{18} column (4.6 × 100 mm, 2 μm particle size) with the above solvent system (solvents A and B) programmed at a flow rate of 0.6 mL min^{-1} and a linear gradient from 0% to 50% B over 25 min. All analogues showed >95% purity when monitored at 220 nm. Molecular weights were checked by a mass spectrometer ESI Micromass ZMD-2000.

Potentiometric measurements

Potentiometric titrations were performed with the following equipments: Orion EA 940 pH meter (resolution 0.1 mV, accuracy 0.2 mV) equipped with a combined glass electrode (Metrohm EA125); Hamilton MicroLab M motor burette (resolution 0.1 μl, accuracy 0.2 μl) equipped with a Hamilton syringe (delivery volume 500 μl). Constant-speed magnetic-stirring was applied throughout. The temperature of the titration cell was kept at 298.2 ± 0.1 K by use of a Haake F3C circulation thermostat. UPP grade nitrogen, previously saturated with H_2O (0.1 M KCl, 298.2 K) was blown over the test solution in order to maintain an inert atmosphere. The electrode couple was standardized on the pH = $-\log c_{H^+}$ scale by titration of HNO_3 (0.01 M) with standard KOH at 298.2 K and I = 0.1 M (KNO_3). Aliquots (2 ml) of sample solution, containing suitable amounts of metal, ligand, HNO_3 and KCl, were titrated with standard KOH. The concentration range employed for both Cu^{2+} ion and the ligands was 0.5–1.1 mM; the ligand : metal ratio was always slightly higher than 1 : 1. The Hyperquad 2006 program[41] was used for stability constant calculations; standard deviations were computed by Hyperquad 2006 and refer to random errors only. Reported $\log\beta$ values refer to the overall equilibria: $pCu + qH + rL = Cu_pH_qL_r$ (the charges omitted); $\log K_{step}$ values refer to the protonation process $Cu_pH_{q-1}L_r + H = Cu_pH_qL_r$ (the charges omitted, p might also be 0). The speciation diagrams were plotted with the Hyss 2006 program.[42]

UV-Vis, EPR and CD measurements

The absorption spectra were recorded on a Cary 300 Bio spectrophotometer. EPR spectra were recorded on a Bruker ESP 300E spectrometer at X-band frequency (9.3 GHz) in liquid nitrogen. The EPR parameters were calculated for the spectra obtained at the maximum concentration of the particular species. Circular dichroism (CD) spectra were recorded on a Jasco J 715 spectropolarimeter in the 800–230 nm range. The values of $\Delta\varepsilon$ (*i.e.*, $\varepsilon_l - \varepsilon_r$) and ε were calculated at the maximum concentration of the particular species obtained from the potentiometric data. Solutions were of similar concentrations to those used in the potentiometric studies; 30% ethylene glycol was used as a cryoprotectant in EPR experiments.

Calorimetric measurements

Enthalpy values for both protonation and Cu^{2+} complexation of the ligands were obtained with calorimetric titrations performed with a Tronac 450 isoperibolic calorimeter equipped with a 3 cm^3 Dewar titration vessel, at T = 298.15 ± 0.02 K and I = 0.1 mol dm^{-3} (KCl). The sample solutions had compositions similar to those employed in potentiometry.

The titrant (standard HNO_3) was added using a 1 cm^3 Hamilton syringe also immersed in the thermostatic bath. The pH range explored was approximately 3–11. A warming resistance ($\sim 100\ \Omega$) and a thermistor placed in the solution, respectively allowed the instrument to be electrically calibrated and temperature variations to be detected. Accuracy was checked daily by titrating a 2-amino-2-(hydroxymethyl)-1,3-propanediol solution with nitric acid. The completely automated system was managed by a personal computer via Tronac 900 interface. The potential difference at thermistor ends was measured by a FLUKE 8840A digital multimeter. Home-made programs for the management of the calorimetric system, data acquisition and gross heat correction for non-chemical contributions[43] and dilution heats (computed from literature data[44]) were all in BASIC language. From experimental ΔH° values the corresponding ΔS° values were computed by means of the Gibbs–Helmholtz equation: $-\Delta G^\circ = -\Delta H^\circ + T\Delta S^\circ$, where the free energy variation was calculated by the corresponding cumulative constants (β), given by potentiometry: $-\Delta G^\circ = 2.303RT\log\beta$.

ΔH° values were computed from the calorimetric data by means of the least-squares computer program HypDH,[45] which minimizes the function: $U = \Sigma w_i(Q_i^o - Q_i^c)^2$, where w_i are statistical weights and Q_i^o, Q_i^c are the experimental and calculated heats, respectively, over n observations. A literature ΔH°_w value of 56.4 kJ mol^{-1}, was used in the calculations.[46]

Throughout, the precision of each thermodynamic parameter is reported as the standard deviation given by the corresponding least-squares program and it is shown in parentheses as uncertainty on the last significant figure.

NMR measurements

Instrumentation. NMR spectra were performed at 9.4 T with a Bruker 400 MHz spectrometer at controlled temperatures (±0.1 K). Solutions were prepared either in 100% D_2O (99.95% from Merck) or in 90% H_2O–10% D_2O mixture, and were carefully deoxygenated through a freezing/vacuum-pumping/sealing/thawing procedure. The pH was adjusted at desired values with either DCl or NaOD and it was corrected for the deuterium effect by considering the following relationship pD = pH + 0.40. The desired concentration of copper ions was achieved by using a stock solution of copper nitrate (Sigma Chemical Co.) in deuterium oxide. TSP-d_4, 3-(trimethylsilyl)-[2,2,3,3-d_4]propanesulfonate, sodium salt, was used as an internal reference standard. Suppression of residual water signal was achieved by presaturation or excitation sculpting. A typical ^{1}H NMR spectrum required 8 transients acquired with a 8 μs 90° pulse, 6600 Hz spectral width, and 2.0 s recycling delay. The assignment was accomplished with TOCSY, COSY, NOESY and ROESY 2D experiments. TOCSY spectra were recorded with a total spin-locking time of 75 ms using a MLEV-17 mixing sequence. Rotating frame Overhauser enhancement spectroscopy (ROESY) was performed at a mixing time ranging from 150 to 300 ms and the radio-frequency strength for the spin-lock field was 1.9 kHz. The spectral width of homonuclear 2D experiments was typically 6000 Hz in both F1 and F2 dimensions. Spin–lattice relaxation rates (R_1) were measured with inversion–recovery pulse sequences. All rates were calculated by regression analysis of the initial recovery curves of longitudinal magnetization components leading to errors not larger than ±3%. While the simple inversion recovery experiment is suitable for the well-isolated peaks, the inversion–recovery sequence applied to TOCSY (IR-TOCSY) was used to calculate the relaxation rates of the overlapping ^{1}H NMR signal. This was obtained by introducing a ^{1}H 180° pulse followed by a variable delay in front of the TOCSY sequence. The T_1 ($= 1/R_1$) values were determined by a three-parameter fit of peak intensities to the following equation:

$$I(\tau) = I_0[1 - (1 + B)\exp(-\tau/T_1)]$$

where B is variable parameter that considers non ideal magnetization and which value is smaller than one. The obtained results were compared with those obtained from normal IR sequence. The agreement was found in the errors limit of both experiments. Spectral processing was performed on a Silicon Graphics O2 workstation using the XWINNMR 3.6 software.

Calculation of the paramagnetic relaxation enhancements. In solutions of peptides containing substoichiometric amounts of paramagnetic ions, the measured spin–lattice relaxation rate was averaged over the values in the free (f) and metal-bound (b) environments:[47]

$$R_{1obs} = \frac{1}{T_{1obs}} = \frac{p_f}{T_{1f} + k_{on}^{-1}} + \frac{p_b}{T_{1b} + k_{off}^{-1}} \qquad (1)$$

where p_f and p_b are fractional populations and k_{on} and k_{off} are kinetic rate constants for entrance into and exit from the metal coordination sphere. Since entrance into the metal coordination sphere, is a fast diffusion controlled process, $k_{on}{}^{-1} \ll T_{1f}$ usually holds, which yields the so-called paramagnetic contribution to the spin–lattice relaxation rate:[48]

$$R_{1b} = R_{1obs} - p_f R_{1f} = \frac{p_b}{T_{1b} + k_{off}^{-1}} \qquad (2)$$

The paramagnetic contribution is easily measured and its uncertainty is strongly related to errors in R_1 measurements (usually not larger than ±3%) and in p_f evaluation (*vide infra*). R_{1p} has the potential of providing $T_{1b} = 1/R_{1b}$, which is the structure-sensitive term and is given by the Solomon equation,[49] here reported for systems with $S = 1/2$:

$$\frac{1}{T_{1b}} = R_{1b} = \frac{1}{10}\left(\frac{\mu_0}{4\pi}\right)^2 \frac{\hbar^2\gamma_I^2\gamma_S^2}{r^6} \times \left\{\frac{\tau_c}{1 + (\omega_I - \omega_S)^2\tau_c^2} + \frac{3\tau_c}{1 + \omega_I^2\tau_c^2} + \frac{6\tau_c}{1 + (\omega_I + \omega_S)^2\tau_c^2}\right\} \qquad (3)$$

where μ is the permeability of vacuum, γ_I and γ_S are the nuclear and electron magnetogyric ratios, respectively, ω_I and ω_S the nuclear and electron Larmor frequencies, r is the metal–nucleus distance, and τ_c is the effective correlation time. The dipole–dipole interaction can be effectively modulated by the electron spin relaxation time, τ_e, or by the rotational

correlation time, τ_R, or by the exchange time, $\tau_M = k_{off}^{-1}$, such that

$$\frac{1}{\tau_c} = \frac{1}{\tau_e} + \frac{1}{\tau_M} + \frac{1}{\tau_R} \quad (4)$$

Since Cu^{2+} has both relatively long electron spin relaxation times in the ns range and the exchange time is usually in the ms to μs range, τ_c is determined by τ_R which, for medium size peptides, is found at values in the 0.5–0.05 ns range or even shorter in the presence of effective internal motions. Since the dependence on r^{-6} limits the error in distances, τ_c was safely approximated by the motional correlation time of the free peptide that, in turn, is either easily calculated from the Stokes equation for all the investigated systems by assuming a hydrodynamic radius equal to 0.16 nm.

When metal–nucleus distances are sought, T_{1b} must be calculated from eqn (2) and, therefore, the k_{off}^{-1} value, if not negligible, must be evaluated. In particular, copper binding to His imidazole always results in the His-Hε···Cu distance fixed at 0.30–0.31 nm independently of N_π or N_τ acting as nitrogen donors. The theoretical values of T_{1b} consistent with these distances were therefore calculated from eqn (3) and inserted in eqn (2) to obtain the k_{off} values.[30,50,51]

Results and discussion

Thermodynamics of protonation and Cu^{2+} complex formation equilibria

All the peptides under investigation are protected at both their C and N ends. The (H96A)$PrP_{92–113}$, (H111A)$PrP_{92–113}$, (H96N$^\tau$-Me-His)$PrP_{92–100}$ and (H111N$^\tau$-Me-His)$PrP_{106–113}$ ligands have been potentiometrically and calorimetrically investigated. The corresponding thermodynamic parameters of protonation are reported in Table 2: they are in good agreement with previous literature data obtained with similar peptides.[31–33,52]

Table 2 Thermodynamic parameters for protonation of $PrP_{92–113}$, $PrP_{92–100}$ and $PrP_{106–113}$ analogues, in aqueous solution; T = 298 K, I = 0.1 mol dm^{-3} (KCl). Standard deviations are given in parentheses. Charges are omitted for clarity

Species	log β	log K_{step}	$-\Delta H°$/kJ mol^{-1}	$\Delta S°$/J K^{-1} mol^{-1}
(H96A)$PrP_{92–113}$				
HL	>11.5		~65	~5
H_2L	21.92(3)	10.42	134(4)	−30(20)
H_3L	32.09(2)	10.17	185(3)	−8(9)
H_4L	41.61(4)	9.52	211(3)	89(9)
H_5L	48.00(6)	6.39	236(3)	127(10)
(H111A)$PrP_{92–113}$				
HL	>11.5		~64	~5
H_2L	21.97(6)	10.47	128(4)	−9(13)
H_3L	32.07(6)	10.10	183(2)	0(7)
H_4L	41.55(8)	9.48	209(2)	94(7)
H_5L	48.01(7)	6.46	245(3)	97(10)
(H96N$^\tau$-Me-His)$PrP_{92–100}$				
HL	6.20(1)		23.8(8)	39(3)
(H111N$^\tau$-Me-His)$PrP_{106–113}$				
HL	10.67(2)		65(2)	−13(7)
H_2L	20.35(2)	9.68	87(2)	96(7)
H_3L	26.31(3)	5.96	108(2)	140(7)

The above PrP fragments are able to bind Cu^{2+}, forming mononuclear complexes of different stoichiometries, depending on the protonation degree of the involved ligand. No bis-complexes have been detected. The presence of a single His residue in these fragments obviously rules out the formation of multi-histidine or dinuclear complexes. The speciation models and the related thermodynamic parameters are reported in Table 3; literature data[31,32] of the corresponding "wild-type" protected peptides $PrP_{91–114}$, $PrP_{92–100}$ and $PrP_{106–113}$ are reported in ESI.† Exemplificative distribution diagrams are shown in Fig. 2. The UV-Vis, CD and EPR spectroscopic results are reported as ESI.†

Experimental results agree that His is always the copper-anchoring site for the first metal-to-ligand interaction at low pH; the log K values corresponding to the equilibrium M + H_4L = MH_4L for the wild-type fragments are close to 4, in very good agreement with the literature log β value for the formation of the 1 : 1 complex of Cu^{2+} with imidazole, under the same experimental conditions.[52] When pH increases neighbouring amido protons can be displaced by the Cu^{2+} ion with the simultaneous coordination of the corresponding peptidic nitrogen and the consequent formation of 2N, 3N and 4N complexes. The most likely binding direction is towards the *N*-terminus, thus involving the His amido-group and forming a six-membered chelation ring. However, the opposite direction is not forbidden, as already discussed in detail in ref. 33. At neutral pH the 3N species is the main complex for the ligands containing His-96 ((H111A)$PrP_{92–113}$ and (H96N$^\tau$-Me-His)$PrP_{92–100}$) while nearly equal amounts of the 3N and 4N complexes are present in the solutions containing (H96A)$PrP_{92–113}$ and (H111N$^\tau$-Me-His)$PrP_{106–113}$ (see Fig. 2). Spectroscopic results referring to the corresponding complex species are very similar for the fragments containing His in the same position (*i.e.* the couples (H96A)$PrP_{92–113}$/(H111N$^\tau$-Me-His)$PrP_{106–113}$ and (H111A)$PrP_{92–113}$/(H96N$^\tau$-Me-His)-$PrP_{92–100}$) confirming that the coordination geometry is conserved, independently of the fragment length, in agreement with Viles *et al.*[22] CD spectra for the systems containing the ligands (H96A)$PrP_{92–113}$ and (H111N$^\tau$-Me-His)$PrP_{106–113}$ are reported in Fig. 3, as an example.

The stoichiometry of the complex species depends on the overall protonation degree of the ligand, due to the presence of Lys side chains, and thus their stability constants cannot be directly compared to each other. An effective way to perform such a comparison is to calculate the corresponding log K* values, where K* refers to the equilibrium:

$$M + LH_n = MLH_j + H_{n-j} \quad (1)$$

where n is the maximum protonation degree of the ligand and j is the protonation degree of the complex; charges are omitted for the sake of simplicity. Values of log K* are shown in Table 4; they confirm that at neutral pH (where 3N and 4N complexes dominate) the His-111 binding site is stronger than the His-96 one, while in the acidic pH range (species 1N and 2N) they are almost equivalent. Long fragments show the same trend as the short ones, suggesting again the same coordination geometry. The influence of the additional amino acidic residues on complex stability is only negligible,

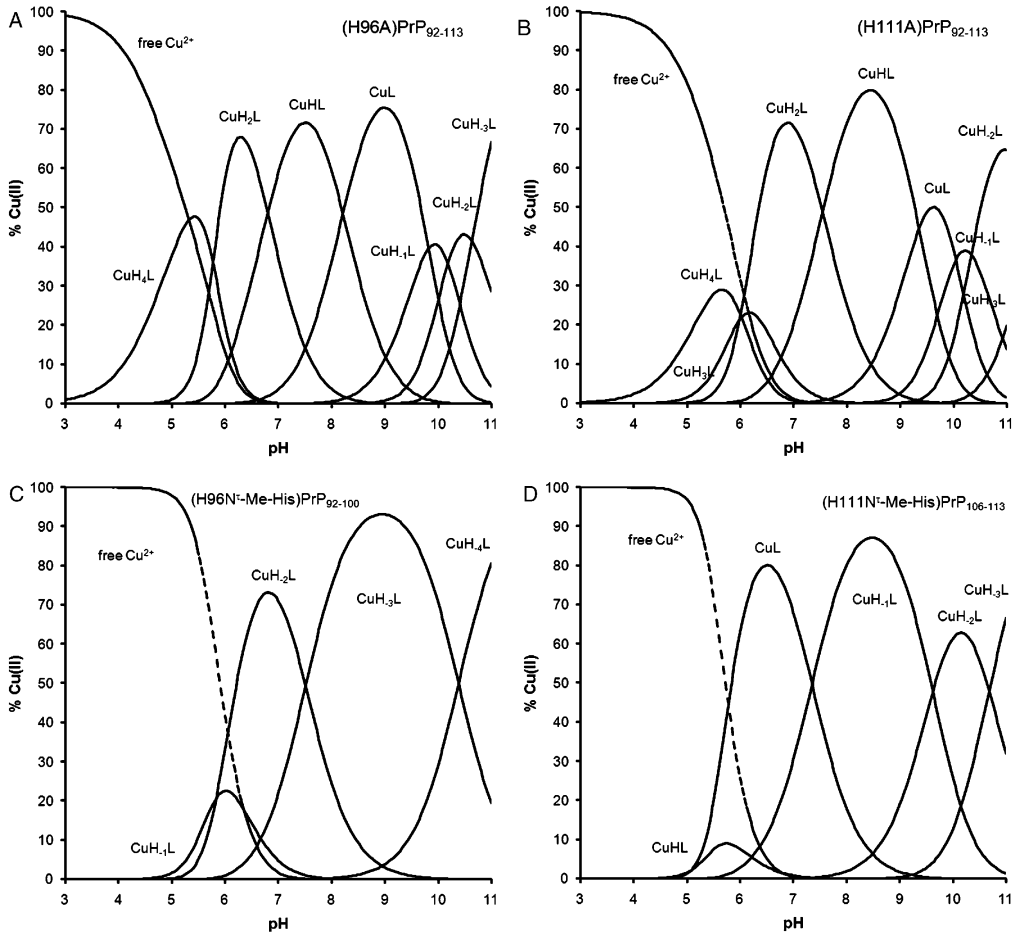

Fig. 2 Exemplificative distribution diagrams for Cu^{2+} complex-formation of PrP_{92-113}, PrP_{92-100} and $PrP_{106-113}$ analogues, in aqueous solution; $[Cu^{2+}] = 1.0$ mM; [ligand] = 1.1 mM.

confirming the preference for the His-111 site over the His-96 one in every case. These findings support our previous results[32] but they disagree with what recently reported by Klewpatinond and Viles[22] who suggested an influence of the hydrophobic *C*-terminal region on the relative Cu^{2+} binding strength of the two His-96 and His-111 sites (see Introduction).

Finally, in the most alkaline pH range, the deprotonation of the unbound τ-nitrogen of His can be suggested for the species $CuH_{-2}L$ formed by (H111A)PrP_{92-113} ($\log K_{step} = 11.51$, Table 3).

NMR investigation on (H96A) and (H111A) substituted peptides

NMR spectra were performed at pH values ranging from 6.5 to 6.8, where the predominance of 3N Cu^{2+} complexes was determined by potentiometric and EPR measurements (*vide supra*). The substitution Ala/His ((H96A)PrP_{92-113}, (H111A)PrP_{92-113}) or the presence of methylated His ((H111N$^{\tau}$-Me-His)PrP_{92-113}, (H96N$^{\tau}$-Me-His)PrP_{92-113}, (H96N$^{\tau}$-Me-His)PrP_{92-100}, (H111N$^{\tau}$-Me-His)$PrP_{106-113}$) yielded NMR spectra very similar to those of the original peptides except for resonances belonging to residues directly involved or close to the inserted modification. Addition of Cu^{2+} affected longitudinal and transverse relaxation rates of protons having a non-vanishing dipolar and/or scalar interaction with the electron spin located at the metal nucleus. As a consequence, proton line broadening allowed to detect residues involved in binding. In both Ala substituted peptides His aromatic protons signals vanished in presence of 0.1 equivalents of Cu^{2+} (Fig. 4) strongly indicating His-96 and His-111 as the main metal anchoring point in (H111A)PrP_{92-113} and (H96A)PrP_{92-113}, respectively. Fig. 4 also shows Trp-99 aromatic proton broadening for the (H111A)PrP_{92-113} system.

Since ^{1}H 1D spectra are too crowded to selectively investigate Cu^{2+} effects on the remainder of the peptides, analysis of IR-TOCSY spectra was preferred to monitor the fastest relaxing protons. Fig. 5A and B show a selected region of the IR-TOCSY spectra of Cu^{2+}–(H96A)PrP_{92-113} and Cu^{2+}–(H111A)PrP_{92-113} systems, respectively. The positive correlations belong to the fastest relaxing protons. In both fragments the largest effects were detected on residues nearby to His; in particular Thr-95, Ser-97 and Gln-98 (in (H111A)PrP_{92-113}) and Met-109, Lys-110, and Met-112 (in (H96A)PrP_{92-113}) exhibited a positive sign. The metal effects on the two fragments were also evaluated by measuring the paramagnetic relaxation enhancement, R_{1p}, reported in Fig. 6. R_{1p} values were obtained from eqn (2) (see Experimental section), assuming that all the added Cu^{2+} (0.1 equiv.) was bound to the peptides ($p_f = 0.9$). Since p_f ranges from 0.9 to 1.0,

Table 3 Thermodynamic parameters for Cu^{2+} complex-formation of $PrP_{92–113}$, $PrP_{92–100}$ and $PrP_{106–113}$ analogues, in aqueous solution; T = 298 K, I = 0.1 mol dm^{-3} (KCl). Standard deviations are given in parentheses. Charges are omitted for clarity

Species	log β	log K_{step}	$-\Delta H^{\circ}$/kJ mol^{-1}	ΔS°/J K^{-1} mol^{-1}
(H96A)$PrP_{92–113}$				
CuH_4L	45.96(4)		200(2)	201(8)
CuH_2L	34.42(3)	6.80	164(2)	103(7)
CuHL	27.62(4)	8.21	129(2)	93(8)
CuL	19.41(6)	9.82	92(2)	61(8)
$CuH_{-1}L$	9.59(7)	10.18	48(4)	20(13)
$CuH_{-2}L$	−0.59(7)	10.63	−12(3)	28(11)
$CuH_{-3}L$	−11.22(8)		n.d.	n.d.
(H111A)$PrP_{92–113}$				
CuH_4L	45.37(3)	6.02	236(3)	80(10)
CuH_3L	39.35(2)	5.98	205(8)	70(27)
CuH_2L	33.37(1)	7.54	173(1)	58(3)
CuHL	25.83(1)	9.35	146(2)	4(7)
CuL	16.48(2)	10.04	118(2)	−80(7)
$CuH_{-1}L$	6.44(2)	10.33	76(3)	−130(10)
$CuH_{-2}L$	−3.89(3)	11.51	5(3)	−90(10)
$CuH_{-3}L$	−15.4(1)		n.d.	n.d.
(H96N$^{\tau}$-Me-His)$PrP_{92–100}$				
$CuH_{-1}L$	−2.58(6)	5.83	0(8)	−50(30)
$CuH_{-2}L$	−8.41(2)	7.51	−42(2)	−21(7)
$CuH_{-3}L$	−15.92(6)	10.38	−69(2)	−74(7).
$CuH_{-4}L$	−26.3(1)		−74(3)	−250(10)
(H111N$^{\tau}$-Me-His)$PrP_{106–113}$				
CuHL	17.54(7)	5.08	92(2)	27(7)
CuL	12.46(1)	7.35	49(2)	76(7)
$CuH_{-1}L$	5.11(3)	9.62	23(2)	21(7)
$CuH_{-2}L$	−4.51(5)	10.68	−6(2)	−65(7)
$CuH_{-3}L$	−15.19(6)		−55(3)	−110(10)

such assumption does not strongly affect the computed R_{1p} values, as shown in Fig. S1 (ESI†) where the R_{1p} values, calculated by using p_f = 1.0 and p_f = 0.9 are compared. Fig. 6 again reveals that the most affected regions are those localized around His residues with the R_{1p} values of Hα of residues either preceding or following His similarly influenced. Moreover the R_{1p} values calculated on the (H111A)$PrP_{92–113}$ system were very similar to those previously detected for the Cu^{2+}–$PrP_{92–100}$ complex[32] suggesting that the 100–113 region does not influence metal binding. This result is in agreement with what was found for His-111 (see above), the copper binding to which is not affected by the presence of the 92–99 region, as shown by CD spectra reported in Fig. 3.

Fig. 6 also shows the R_{1p} values previously reported[32] for the wild $PrP_{92–113}$ fragment. The agreement with the (H111A)$PrP_{92–113}$ and (H96A)$PrP_{92–113}$ systems is very good, with the only a minor difference on the absolute values, probably due to the difference in the applied magnetic field. The metal effects detected on $PrP_{92–113}$ were localized in the proximity of the two His: the residues preceding and following the two imidazoles exhibited the largest R_{1p} thus confirming that both histidines can bind a Cu^{2+} ion. In particular, (i) the (H96A)$PrP_{92–113}$ fragment had paramagnetic effects very similar to the wild-type peptide except for Ala-113 protons which were completely overlapped with Ala-96 resonances in the NMR spectra and (ii) the paramagnetic effects recorded on (H111A)$PrP_{92–113}$ fragment were larger than those of $PrP_{92–113}$, although exhibiting a similar behavior.

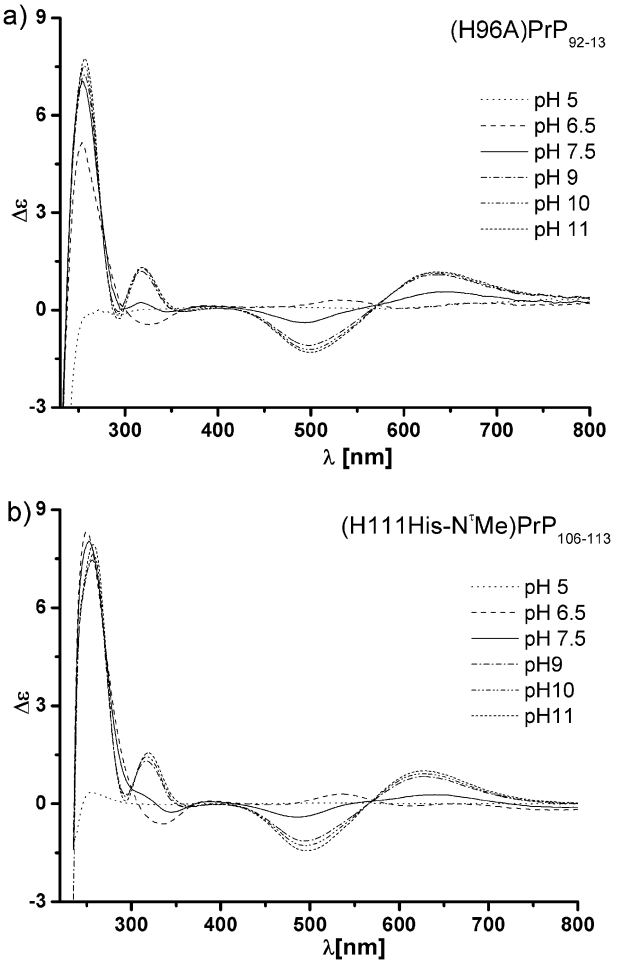

Fig. 3 CD spectra of (a) Cu^{2+}/(H96A)PrP_{92-113} and (b) Cu^{2+}/(H111N$^{\tau}$-Me-His)$PrP_{106-113}$ as 1.0/1.1 mM solutions at different pH values.

Table 4 log K^* data (see text) for Cu^{2+} complex-formation of PrP fragments and analogues

Species	1N	2N	3N	4N
(H111A)$PrP_{92–113}$	−2.64	−8.66	−14.64	−22.18
(H96N$^{\tau}$-Me-His)$PrP_{92–100}$	—	−8.78	−14.61	−22.12
$PrP_{92–100}$[a]	−2.53	−8.78	−14.60	−22.15
(H96A)$PrP_{92–113}$	−2.04	—	−13.58	−20.38
(H111N$^{\tau}$-Me-His)$PrP_{106–113}$	—	−8.77	−13.85	−21.20
$PrP_{106–113}$[b]	−2.64	−8.63	−13.87	−21.58

[a] Data from ref. 32. [b] Data from ref. 31.

These findings suggest that: (i) copper binding modes at His-111 or His-96 site are independent from each other, in agreement with Osz *et al.*[36] and Viles *et al.*;[23] (ii) Cu^{2+} does not equally distribute between the two His sites and only a very small metal amount interacts with His-96 in the original peptide, indicating His-111 as the preferred metal binding site in the full length $PrP_{92–113}$ fragment, as already deduced from thermodynamic results discussed above, and in agreement with most of literature (see Introduction). However, it is worth noting that Viles *et al.*[22] suggested that at pH 6.5 and at low Cu^{2+} equivalents (0.1–0.2), metal binding to $PrP_{90–126}$ can

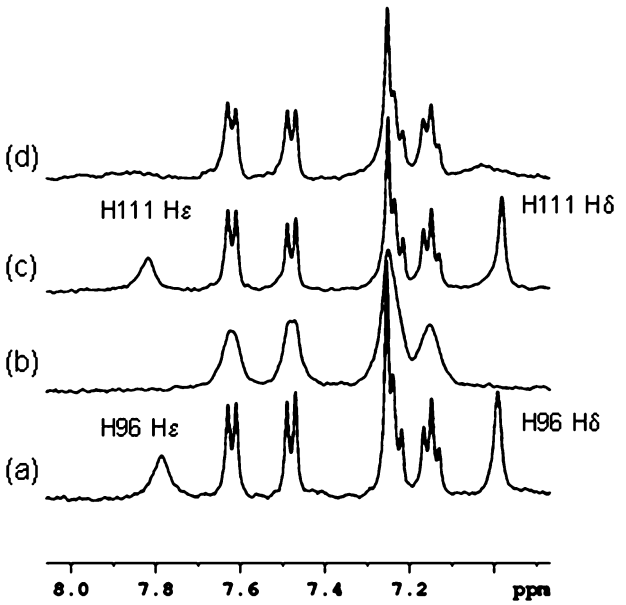

Fig. 4 ^{1}H NMR aromatic region spectra of (H111A)PrP$_{92\text{-}113}$ and (H96A)PrP$_{92\text{-}113}$; 2.5 mM, pH 6.5, T = 298 K in the absence (traces (a) and (c), respectively) and in the presence of 0.1 equivalents of Cu^{2+} (traces (b) and (d), respectively).

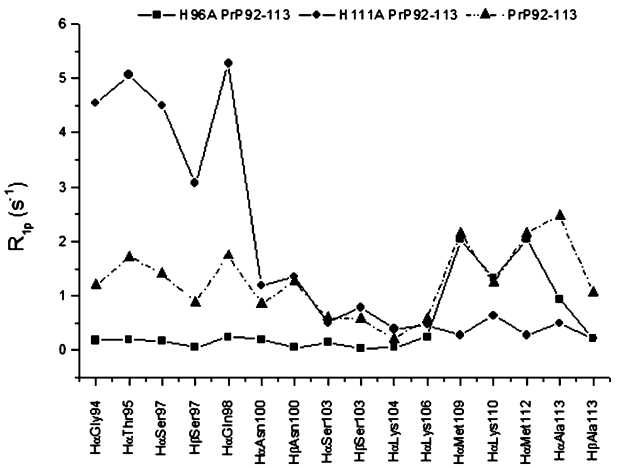

Fig. 6 Proton paramagnetic relaxation contributions (R_{1p}) of (H96A)PrP$_{92\text{-}113}$ (squares), (H111A)PrP$_{92\text{-}113}$ (circles) and PrP$_{92\text{-}113}$ (triangles) calculated in the presence of 0.1 equivalents of Cu^{2+}; T = 298 K, pH 6.5.

involve both His-96 and His-111 side-chains, with the formation of a 2N2O complex, different from the species (3NO) observed at metal : ligand ratios larger than 0.4 and at neutral pH. In the present study, the absence of His-96 or His-111 in the (H96A)PrP$_{92\text{–}113}$ and (H111A)PrP$_{92\text{–}113}$ fragments rules out the existence of a multiple histidine binding mode unless the formation of two different bis-complexes, one centered on His-96 and the other on His-111, is suggested. However, this looks very unlikely in the wild-type PrP$_{92\text{–}113}$ fragment, because such a behaviour would result in slower τ_c, different k_{off} and p_f, strongly affecting the R_{1p} values. On the contrary, (H96A)PrP$_{92\text{–}113}$ and PrP$_{92\text{–}113}$ exhibited very similar R_{1p} values (Fig. 6) and this result is consistent only with the presence of the same copper binding sites. Moreover, any bis-complex eventually formed in significant amount would have been detected by potentiometry even at equimolar Cu^{2+} ratio, but this was never the case.

Proton paramagnetic relaxation enhancements of His-96 and His-111 aromatic protons of (H111A) and (H96A)PrP$_{92\text{–}113}$ complexes were also measured, in order to evaluate whether N^{π} or N^{τ} was the donor atom. The measured R_{1p} were used to obtain the k_{off} values and His H$\delta\cdots Cu^{2+}$ distances in the two copper complexes (Table 5). The obtained distances, 0.45 nm for both His, are in agreement with copper binding to N^{π} rather than N^{τ}. The same Cu^{2+} coordinated nitrogen was

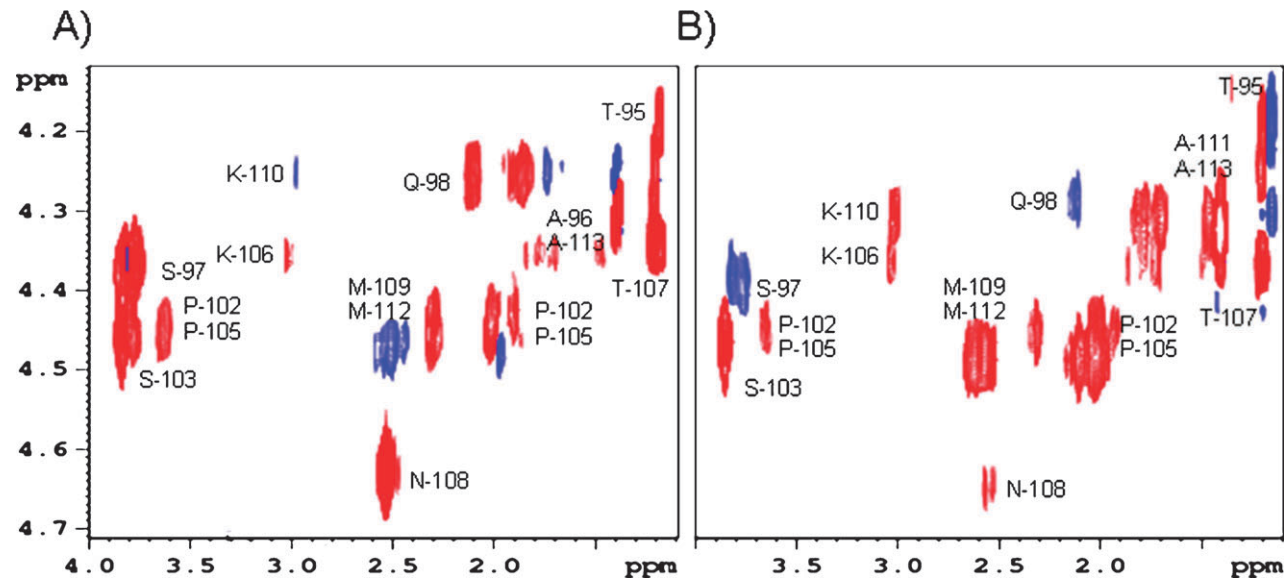

Fig. 5 ^{1}H–^{1}H 2D maps from IR-TOCSY experiments performed with $d1$ = 5 s, t = 0.4 s showing negative (red) and positive (blue) cross-peaks. Positive correlations correspond to the fastest relaxing resonances. (A) (H96A)PrP$_{92\text{-}113}$: only residues near by His-111 (Lys-110, Met-109 and Ala-113) are affected. (B) (H111A)PrP$_{92\text{-}113}$: only residues near by His-96 (Thr-95, Ser-97 and Gln-98) are affected.

Table 5 Paramagnetic relaxation contributions (R_{1p}), exchange rate values (k_{off}) and copper distances (r) for imidazole protons of Cu^{2+}–(H111A) and Cu^{2+}–(H96A)$PrP_{92–113}$ complexes, at T = 298 K

	+0.01 eq. Cu^{2+}			+0.02 eq. Cu^{2+}			+0.05 eq. Cu^{2+}		
	R_{1p}/s^{-1}	r/nm	k_{off}/ms^{-1}	R_{1p}/s^{-1}	r/nm	k_{off}/ms^{-1}	R_{1p}/s^{-1}	r/nm	k_{off}/ms^{-1}
(H111A)$PrP_{92–113}$									
Hε His-96	13.8	0.30	1.5	28.2	0.31	1.5	n.d[a]		
Hδ His-96	8.7	0.44		16.3	0.45		n.d[a]		
(H96A)$PrP_{92–113}$									
Hε His-111	8.2	0.30	0.9	16.5	0.30	0.9	34.2	0.30	0.7
Hδ His-111	5.7	0.45		12.7	0.42		22.7	0.48	

[a] The resonances are so broad so as to prevent the measurement of the relaxation rates.

pointed out by other investigations on Cu^{2+} complexes with fragments containing His-96, His-111 or both,[32,33] suggesting that Ala substitutions does not affect the Cu^{2+} binding modes. Moreover the different R_{1p} values of His Hε and Hδ calculated for the two Ala substituted systems, support the presence of 1 : 1 metal complexes, since paramagnetic effects independent of the His position are expected in the case of multiple His metal binding.

NMR investigation on peptides containing N^{τ}-Me-His

It was previously reported that the τ-nitrogens of imidazole side chains of His residues are not directly involved in metal coordination.[31–33] Actually, methylation of His in (H96N^{τ}-Me-His)$PrP_{92–100}$ and (H111N^{τ}-Me-His)$PrP_{106–113}$ leaves unchanged the complex formation behaviour of both the copper-binding sites (see Table 3, Table 4, Fig. 3 and ESI†). The unique difference concerns the anchoring ability of His at the most acidic pH values, as it can be easily deduced by the distribution diagrams in Fig. 2: His methylation moves the formation of the first complex species from pH 3.5 to 5.0. At acidic pH both the nitrogen atoms of imidazole ring of His are protonated and they are nearly equivalent from the acid–base point of view. However, N^{τ} is more exposed to the solution bulk and thus to the interaction with copper ions. Methylation makes N^{τ} unavailable and it also hinders the approaching of metal ions to the other imidazole nitrogen. As a consequence, only negligible amounts of 1N complex are formed; complex-formation really starts only when the pH value is sufficiently high to allow the displacement of one or more amido hydrogens by Cu^{2+}, the peptide acting as a bidentate or tridentate ligand.

The presence of one methylated His resulted in a relatively large ppm difference between the His-96 and His-111 aromatic protons (Fig. 7). The obtained chemical-shift separation allowed to selectively measure the Cu(II) effects on His-96 and His-111 in (H96N^{τ}-Me-His)$PrP_{92–113}$ and (H111N^{τ}-Me-His)-$PrP_{92–113}$ analogues, contrarily to what found for the system containing the wild-type $PrP_{91–114}$ or $PrP_{91–120}$ peptides.[32] The measured paramagnetic effects (R_{1p}) are shown in Table 6 and Fig. 8, together with the corresponding $PrP_{92–113}$ values. Fig. 8 (upper) indicates that the N^{τ} methylation of His-96 does not significantly affect the R_{1p} behavior, with the observed trends almost identical to those of the original peptide, and exhibiting the largest effects on the proximity of the two His. Such comparison, however, shows that the R_{1p} absolute values are not identical. On the other hand the comparison, performed on the $PrP_{92–113}$ and the corresponding (H111N^{τ}-Me-His) analogues (Fig. 8, lower) revealed comparable R_{1p} effects for the His-96 site while N^{τ} unavailability causes large changes of R_{1p} values for the His-111 site. The different behavior of (H96N^{τ}-Me-His)$PrP_{92–113}$ or (H111N^{τ}-Me-His)$PrP_{92–113}$ peptides could be explained by considering that His-111 is the favored metal anchoring point and its methylation could yield more important changes than those of His-96, which on the contrary exhibited smaller changes because of the low metal occupancy. The occurrence of multi His species was excluded also for these systems. In fact, the measured copper binding effects of smaller fragments ((H96N^{τ}-Me-His)-$PrP_{92–100}$ and H111N^{τ}-Me-His)$PrP_{106–113}$) were comparable to those of (H96N^{τ}-Me-His)$PrP_{92–113}$ or (H111N^{τ}-Me-His)-$PrP_{92–113}$ (see ESI†).

Since potentiometry, UV-Vis, CD and EPR spectroscopy and calorimetric studies have shown that N^{τ} methylation does not yield any changes in the Cu^{2+} complexes with the investigated peptides (see above), the different R_{1p} values of (H111N^{τ}-Me-His)$PrP_{92–113}$ could be due to (i) different kinetic processes, (for example, the transition state model may be consistent with crossing different transition state, depending on the presence of normal or N^{t}-methylated His), (ii) slower reorientational correlation times derived from a larger sterical hindrance of the methylated His, and (iii) the occurrence of different paramagnetic contributions.

Moreover the interpretation of the paramagnetic contributions is usually complicated by many other factors such as (i) the formation of minor and weak rapidly exchange copper species which could have a profound effect on ^{1}H NMR relaxation of nearby protons and (ii) the proximity of flexible parts of the

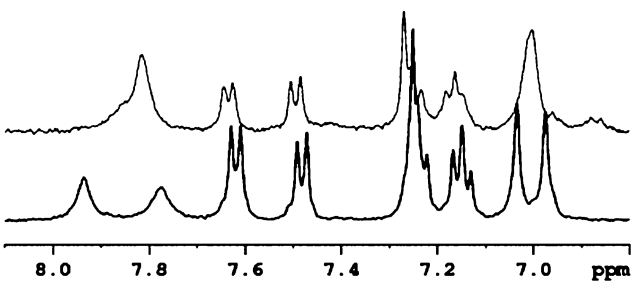

Fig. 7 ^{1}H NMR aromatic region spectra of PrP_{92-113} (upper trace) and (H96N^{τ}-Me-His)PrP_{92-113} (lower trace); 2.5 mM, pH 6.5, T = 298.

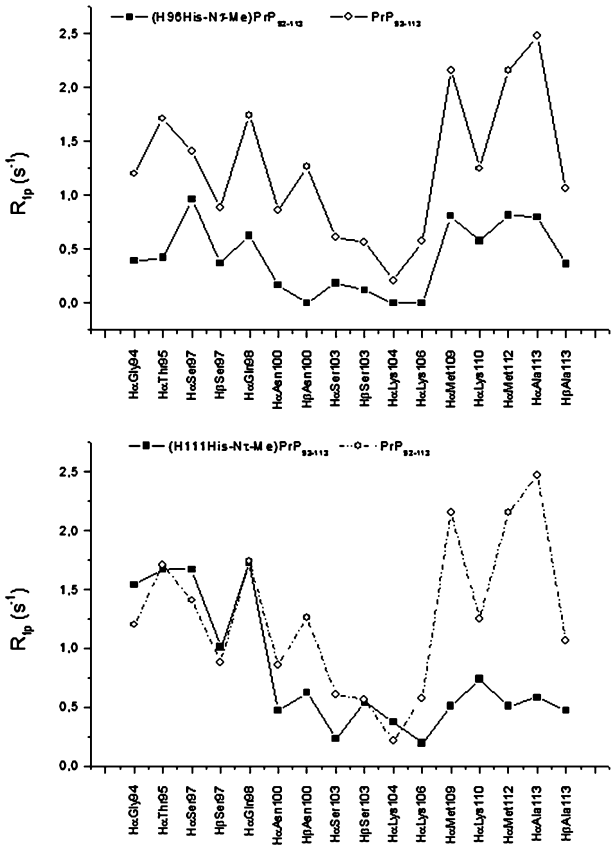

Fig. 8 Comparison between proton paramagnetic relaxation contributions (R_{1p}) of $PrP_{92\text{-}113}$ and (H96His-N^{τ}-Me)$PrP_{92\text{-}113}$ (upper) or (H111His-N^{τ}-Me)$PrP_{92\text{-}113}$ (lower) calculated in the presence of 0.1 equivalents of Cu^{2+}; T = 298 K, pH 6.5.

Table 6 ^{1}H R_{1p} (s^{-1}) of (H111N^{τ}-Me-His)$PrP_{92\text{–}113}$ and (H96N^{τ}-Me-His)$PrP_{92\text{–}113}$; 2.5 mM, pH = 6.5

(H111N^{τ}-Me-His)$PrP_{92\text{–}113}$ + 0.05 eq. Cu^{2+}			
	Hε	Hδ	Me
His-96	12.7	11.0	
His-111	9.72	0.80	0.39
(H96N^{τ}-Me-His)$PrP_{92\text{–}113}$ + 0.1 eq. Cu^{2+}			
	Hε	Hδ	Me
His-96	6.77	0.62	0.24
His-111	9.50	5.53	

peptide main-chain to the Cu^{2+} centre for brief periods of time which could also experience significant relaxation.

Conclusions

It is now widely accepted that PrP^{C} is a copper-binding protein which plays a role in copper homeostasis. Much attention has been devoted in last decade to the octameric sequence PHGGWGQ and its four repetitions contained in the N-terminal domain of PrP^{C}, since this region has been first recognized as capable to bind up to four Cu^{2+} ions. The location of the "fifth binding site" at His-96 and/or His-111, again in the *N*-terminal unstructured domain of PrP^{C}, as been only recently proposed and its copper-binding features have not been fully elucidated yet. In the present paper, some peptidic analogues of the $PrP_{92\text{–}113}$ fragment of human PrP^{C} have been employed to clarify the role of the two His residues and their coordination modes to Cu^{2+} ion. The results confirmed that His-111 and His-96 act as independent binding sites, even at Cu^{2+}-ion substoichiometric levels, the former being stronger than the latter. Neither multi-histidine binding nor bis-complex formation has been detected at neutral pH. Their N^{τ} methylation does not substantially modify the copper-binding behavior: the τ nitrogen of the imidazole side chain can participate in complex-formation only at acidic pH, where displacement of amidic protons by Cu^{2+} ions is not allowed. Finally, the length of the fragment does not appear to have any significant influence on the behavior of the two His-96 and His-111 binding sites, from the point of view of either the coordination geometry or their relative strength.

Table of abbreviations

hPrP	Human Prion Protein
IR-TOCSY	Inversion Recovery-TOtal Correlated SpectroscopY
mPrP	Mouse Prion Protein
NOE	Nuclear Overhauser Effect
NOESY	NOE SpectroscopY
PrP^{C}	Normal Prion Protein
PrP^{Sc}	Abnormal isoform of Prion Protein (Scrapie form)
ROESY	Rotating frame Overhauser Effect SpectroscopY
SOD	Super Oxide Dismutase
TOCSY	TOtal Correlated SpectroscopY
TSE	Transmissible Spongiform Encephalopathy
XAS	X-ray Absorption Spectroscopy

Acknowledgements

We would like to acknowledge the CIRMMP (Consorzio Interuniversitario Risonanze Magnetiche di Metalloproteine Paramagnetiche), the University of Ferrara and the MIUR (FIRB RBNE03PX83_003) and Polish Ministry of Science and Higher Education (N N204 340637) for financial support.

References

1 S. B. Prusiner, *Proc. Natl. Acad. Sci. U. S. A.*, 1998, **95**, 13363–13383.
2 S. B. Prusiner, *Science*, 1997, **278**, 245–251.
3 R. G. Will, J. W. Ironside, M. Zeidler, S. N. Cousens, K. Estibeiro, A. Alperovitch, S. Poser, M. Pocchiari, A. Hofman and P. G. Smith, *Lancet*, 1996, **347**, 921–925.
4 T. Blattler, *APMIS*, 2002, **110**, 71–78.
5 P. Davies and D. R. Brown, *Biochem. J.*, 2008, **410**, 237–244.
6 E. Gaggelli, H. Kozlowski, D. Valensin and G. Valensin, *Chem. Rev.*, 2006, **106**, 1995–2044.
7 D. R. Brown and H. Kozlowski, *Dalton Trans.*, 2004, 1907–1917, and references therein.
8 F. Wopfner, G. Weidenhofer, R. Schneider, A. von Brunn, S. Gilch, T. F. Schwarz, T. Werner and H. M. Schatzl, *J. Mol. Biol.*, 1999, **289**, 1163–1178.
9 E. Rivera-Milla, C. A. O. Stuermer and E. Malaga-Trillo, *Trends Genet.*, 2003, **19**, 72–75.

10 D. R. Brown, K. Qin, J. W. Herms, A. Madlung, J. Manson, R. Strome, P. E. Fraser, T. Kruck, A. von Bohlen, W. Schulz-Schaeffer, A. Giese, D. Westaway and H. Kretzschmar, *Nature*, 1997, **390**, 684–687.
11 G. S. Jackson, I. Murray, L. L. P. Hosszu, N. Gibbs, J. P. Waltho, A. R. Clarke and J. Collinge, *Proc. Natl. Acad. Sci. U. S. A.*, 2001, **98**, 8531–8535.
12 S. S. Hasnain, L. M. Murphy, R. W. Strange, J. G. Grossmann, A. R. Clarke, G. S. Jackson and J. Collinge, *J. Mol. Biol.*, 2001, **311**, 467–473.
13 M. A. Wells, G. S. Jackson, S. Jones, L. L. P. Hosszu, C. J. Craven, A. R. Clarke, J. Collinge and J. P. Waltho, *Biochem. J.*, 2006, **399**, 435–444.
14 C. S. Burns, E. Aronoff-Spencer, G. Legname, S. B. Prusiner, W. E. Antholine, G. J. Gerfen, J. Peisach and G. L. Millhauser, *Biochemistry*, 2003, **42**, 6794–6803.
15 C. E. Jones, S. R. Abdelraheim, D. R. Brown and J. H. Viles, *J. Biol. Chem.*, 2004, **279**, 32018–32027.
16 C. E. Jones, M. Klewpatinond, S. R. Abdelraheim, D. R. Brown and J. H. Viles, *J. Mol. Biol.*, 2005, **346**, 1393–1407.
17 A. R. Thompsett, S. R. Abdelraheim, M. Daniels and D. R. Brown, *J. Biol. Chem.*, 2005, **280**, 42750–42758.
18 M. A. Wells, C. Jelinska, L. L. P. Hosszu, C. J. Craven, A. R. Clarke, J. Collinge, J. P. Waltho and G. S. Jackson, *Biochem. J.*, 2006, **400**, 501–510.
19 G. L. Millhauser, *Annu. Rev. Phys. Chem.*, 2007, **58**, 299–320.
20 M. Chattopadhyay, E. D. Walter, D. J. Newell, P. J. Jackson, E. Aronoff-Spencer, J. Peisach, G. J. Gerfen, B. Bennett, W. E. Antholine and G. L. Millhauser, *J. Am. Chem. Soc.*, 2005, **127**, 12647–12656.
21 D. Valensin, M. Luczkowski, F. M. Mancini, A. Legowska, E. Gaggelli, G. Valensin, K. Rolka and H. Kozlowski, *Dalton Trans.*, 2004, 1284–1293.
22 M. Klewpatinond and J. H. Viles, *Biochem. J.*, 2007, **404**, 393–402.
23 M. Klewpatinond, P. Davies, S. Bowen, D. R. Brown and J. H. Viles, *J. Biol. Chem.*, 2008, **283**, 1870–1881.
24 C. Treiber, A. R. Thompsett, R. Pipkorn, D. R. Brown and G. Multhaup, *JBIC, J. Biol. Inorg. Chem.*, 2007, **12**, 711–720.
25 J. Shearer and P. Soh, *Inorg. Chem.*, 2007, **46**, 710–719.
26 J. Shearer, P. Soh and S. Lentz, *J. Inorg. Biochem.*, 2008, **102**, 2103–2113.
27 J. B. Pollock, P. J. Cutler, J. M. Kenney, P. J. Gemperline and C. S. Burns, *Anal. Biochem.*, 2008, **377**, 223–233.
28 R. Srikanth, J. Wilson, C. S. Burns and R. W. Vachet, *Biochemistry*, 2008, **47**, 9258–9268.
29 B. Belosi, E. Gaggelli, R. Guerrini, H. Kozłowski, M. Łuczkowski, F. M. Mancini, M. Remelli, D. Valensin and G. Valensin, *ChemBioChem*, 2004, **5**, 349–359.
30 E. Gaggelli, F. Bernardi, E. Molteni, R. Pogni, D. Valensin, G. Valensin, M. Remelli, M. Luczkowski and H. Kozlowski, *J. Am. Chem. Soc.*, 2005, **127**, 996–1006.
31 M. Remelli, M. Donatoni, R. Guerrini, A. Janicka, P. Pretegiani and H. Kozlowski, *Dalton Trans.*, 2005, 2876–2885.
32 F. Berti, E. Gaggelli, R. Guerrini, A. Janicka, H. Kozlowski, A. Legowska, H. Miecznikowska, C. Migliorini, R. Pogni, M. Remelli, K. Rolka, D. Valensin and G. Valensin, *Chem.–Eur. J.*, 2007, **13**, 1991–2001.
33 E. Gralka, D. Valensin, E. Porciatti, C. Gajda, E. Gaggelli, G. Valensin, W. Kamysz, R. Nadolny, R. Guerrini, D. Bacco, M. Remelli and H. Kozlowski, *Dalton Trans.*, 2008, 5207–5219.
34 G. Di Natale, G. Grasso, G. Impellizzeri, D. La Mendola, G. Micera, N. Mihala, Z. Nagy, K. Osz, G. Pappalardo, V. Rigó, E. Rizzarelli, D. Sanna and I. Sóvágó, *Inorg. Chem.*, 2005, **44**, 7214–7225.
35 V. Jószai, Z. Nagy, K. Osz, D. Sanna, G. Di Natale, D. La Mendola, G. Pappalardo, E. Rizzarelli and I. Sóvágó, *J. Inorg. Biochem.*, 2006, **100**, 1399–1409.
36 K. Osz, Z. Nagy, G. Pappalardo, G. Di Natale, D. Sanna, G. Micera, E. Rizzarelli and I. Sóvágó, *Chem.–Eur. J.*, 2007, **13**, 7129–7143.
37 K. Osz, *J. Inorg. Biochem.*, 2008, **102**, 2184–2195.
38 G. Di Natale, K. Osz, Z. Nagy, D. Sanna, G. Micera, G. Pappalardo, I. Sovago and E. Rizzarelli, *Inorg. Chem.*, 2009, **48**, 4239–4250.
39 L. A. Carpino and G. Y. Han, *J. Org. Chem.*, 1972, **37**, 3404–3409.
40 N. A. Solé and G. Barany, *J. Org. Chem.*, 1992, **57**, 5399–5403.
41 P. Gans, A. Sabatini and A. Vacca, *Talanta*, 1996, **43**, 1739–1753.
42 L. Alderighi, P. Gans, A. Ienco, D. Peters, A. Sabatini and A. Vacca, *Coord. Chem. Rev.*, 1999, **184**, 311–318.
43 L. D. Hansen, T. E. Jensen, S. Mayne, D. J. Eatough, R. M. Izatt and J. J. Christensen, *J. Chem. Thermodyn.*, 1975, **7**, 919–926.
44 *CRC Handbook of Chemistry and Physics*, ed. D. R. Lide, CRC Press, London, 77th edn, 1996, ch. 5, p. 107.
45 P. Gans, A. Sabatini and A. Vacca, *J. Solution Chem.*, 2008, **37**, 467–476.
46 A. Vacca, A. Sabatini and L. Bologni, *J. Chem. Soc., Dalton Trans.*, 1981, 1246–1250.
47 I. Bertini and C. Luchinat, *Coord. Chem. Rev.*, 1996, **150**, 1–292; I. Bertini and C. Luchinat, *Coord. Chem. Rev.*, 1998, **170**, 283–288.
48 L. Banci, I. Bertini and C. Luchinat, *Nuclear and Electron Relaxation*, VCH, Weinheim, Germany, 1991.
49 I. Solomon, *Phys. Rev.*, 1955, **99**, 559–565.
50 E. Gaggelli, N. D'Amelio, D. Valensin and G. Valensin, *Magn. Reson. Chem.*, 2003, **41**, 877–883.
51 E. Gaggelli, H. Kozłowski, D. Valensin and G. Valensin, *Mol. BioSyst.*, 2005, **1**, 79–84.
52 L. D. Pettit and H. K. J. Powell, *The IUPAC Stability Constants Database*, London, UK, 1992–2002.

